Vacuum 227 (2024) 113395

Contents lists available at ScienceDirect

Vacuum

journal homepage: www.elsevier.com/locate/vacuum

Exploring electron energy dependencies in the formation of surface charge on ZnO crystals

Utkirjon Sharopov [a,b,*], Kamoliddin Samiev [b], Akbarjon To'raev [b], Muzaffar Kurbanov [c], Mukhtorjon Karimov [c], Dilmurod Saidov [d], Feruza Akbarova [e], Sitora Turopova [e], Zafar Iskandarov [f], Sokhib Islamov [f], Aleksei Komolov [j], Igor Pronin [h], Hanna Bandarenka [i], Odiljon Abdurakhmonov [k], Sherzod Abdurakhmonov [l], Marutheeswaran Srinivasan [g], Kulwinder Kaur [m]

[a] Physical-Technical Institute, Uzbekistan Academy of Sciences, Tashkent, Uzbekistan
[b] Bukhara State University, Bukhara, Uzbekistan
[c] Urgench State University, Urgench, Uzbekistan
[d] Urgench Branch of the Tashkent University of Information Technologies, Urgench, Uzbekistan
[e] Institute of Materials Science, Tashkent, Uzbekistan
[f] Tashkent State Agrarian University, Tashkent, Uzbekistan
[j] St Petersburg State University, St Petersburg, Russia
[h] Penza State University, Penza, Russia
[i] Belarusian State University of Informatics and Radioelectronics, Minsk, Belarus
[g] Tashkent Institute of Chemical Technology, Tashkent, Uzbekistan
[k] Almalyk Branch, National University of Science and Technology MISIS, Almalyk, Uzbekistan
[l] School of Physical Sciences, Amrita Vishwa Vidyapeetham, Mysuru, India
[m] Mehr Chand Mahajan, DAV College for Women, 160036, Chandigarh, India

ARTICLE INFO

Handling Editor: Prof. L.G. Hultman

Keywords:
Zinc oxide
Charge
Surface
Electron irradiation
Temperature annealing
Defect formation

ABSTRACT

This study delves into the phenomena surrounding the emergence of negative charge accumulation on the surface of zinc oxide (ZnO) crystals upon exposure to low-energy electron irradiation within the range of E = 0 ÷ 600 eV. We demonstrate the critical significance of the primary electron energy in dictating the initial processes initiated at the ZnO surface. Energy thresholds governing both the genesis and elimination of surface charge, along with the formation of oxygen vacancies on the ZnO surface, are elucidated. Our findings reveal that irradiation instigates distinct dissociative pathways contingent upon electron energy, engendering diverse physical and chemical transformations via bond dissociation, desorption, and atomic and molecular restructuring of the surface. These insights serve as pivotal groundwork towards advancing the fabrication of epitaxial films, facilitating the controlled generation of two-dimensional structures predicated on surface potential modulation.

1. Introduction

Surface charging phenomena under electron irradiation are pivotal in understanding the dynamic interactions between electron beams and materials, especially in the fields of materials science, nanotechnology, and electron microscopy [1]. When a material is exposed to an electron beam, the incident electrons can be absorbed, transmitted, or reflected by the material's surface, leading to the accumulation of electrical charge [2]. This process is influenced by the material's conductivity, electron affinity, and the energy of the incident electrons. Surface charging can significantly affect the physical and chemical properties of the material, leading to various applications and implications in scientific research and industrial applications.

As we all know, protons and electrons are the basis of catalysis processes [3,4]. Depending on the energy value, electrons, interacting with molecules, can stimulate various desorption [5] and dissociative processes [6–8]. The predominance of one process over another depends on the energy of the electron [9]. Therefore, electron energy is

* Corresponding author. "Solar thermal and power plants" laboratory, Physical-Technical Institute, Chingiz Aitmatov St.2, 100084, Tashkent, Uzbekistan.
E-mail address: utkirstar@gmail.com (U. Sharopov).

https://doi.org/10.1016/j.vacuum.2024.113395
Received 24 March 2024; Received in revised form 10 June 2024; Accepted 12 June 2024
Available online 14 June 2024

extremely important for revealing models and mechanisms of various processes [10]. However, the process of determining the threshold of various mechanisms is very difficult in the condensed phase, since multiple scattering leads to the formation of reaction cascades (for example, desorption, dissociation, charging, the formation of radiolysis products, recombination, etc.). The advantage of low-energy electrons is that (0–100 eV) it is possible to highlight the transition boundaries of processes, including the control of surface chemistry processes, in which a large number of secondary electrons are observed. The formation of negative and positive particles on the surface is also important, in addition to the fact that research on them is rather scarce, since these processes cover most of the expected dissociative processes, as well as the processes of synthesis of new molecules, desorption and sputtering [11]. In real systems, everything is not so simple and to establish the contribution to the observed chemical activity, in the low-energy regime we can isolate, prioritize and carefully study these individual processes.

In our work on the study of surface states, we discovered charging of the surface of semiconductors and dielectrics (ZnO, LiF, CuO) upon irradiation with low-energy primary electrons [12,13]. Domestic and foreign works have shown that this phenomenon with the energy of primary electrons below 100 eV has not been studied [14].

Since the ZnO crystal is a promising material and is very actively studied due to its optical and luminescent properties [15–17], we needed interest in the phenomenon of charging the surface of ZnO crystals when irradiated with electrons with an energy of 1–1000 eV by the method of total current spectroscopy to understand the structure of electronic states and the nature of chemical bonds on the surface of zinc oxide. This phenomenon of secondary electron emission [18] from ionic crystals and the accompanying charging effect when exposed to electron radiation has been studied for many years [19], but many aspects of this multifaceted phenomenon are still not understood and require further research [20]. Based on the latter circumstance, we can say that the study of problems of charging the surface of crystals has not only scientific, but also a lot of practical significance, for example, for analytical electron probe research techniques [21–23], electron lithography [24], and optoelectronic technology [25], in many modern space technologies [26–29]. Among Si [30], GaN, ZnO [31], SiO_2 [32], TiO_2, InP [33] and GaP etc; Zinc oxide has wide band gap (3.37 eV), large exciton binding energy and is radiation resistive [34]. Because of these instrinsic properties ZnO has been applied in detection of UV radiation, space communications [35], pollution, water purification, defense applications [36,37].

This manuscript investigates the mechanisms governing surface charge accumulation in polycrystalline and single-crystal zinc oxide (ZnO) under electron irradiation. The emphasis lies on elucidating the fundamental physical processes involved, exploring the factors that influence charging behavior, and outlining strategies to mitigate associated undesirable effects. By offering a critical analysis of recent advancements and highlighting the remaining challenges, this work aims to contribute to a deeper understanding of electron-material interactions within ZnO. This knowledge will pave the way for the development of novel methodologies to control and harness surface charge across diverse scientific and technological domains, including the potential exploitation of negative surface charge for the targeted growth of crystals and films. Previously, using total current spectroscopy [38], we studied the energy dependences of defect formation in ZnO crystals [12]. This paper presents the results of a further study of the kinetics and temperature dependences of the formation of negative charging and defects on the ZnO surface under electron irradiation. The thresholds for charge formation were determined and an attempt was made to explain the mechanisms of the ongoing physical process. These physical processes underlying defects on the surface are so important that their study leads to the improvement of zinc oxide coatings for use in spacecraft [29], photodetectors, and diode emitters in the ultraviolet region [39].

2. Materials and experimental methods

The experiments used ultrapure single crystals and polycrystals of zinc oxide grown by explosive laser deposition on sapphire (Al_2O_3) substrates. Zinc oxide single crystals were grown by the hydrothermal method in Germany, orientation (000 $\bar{1}$), dimensions 10 × 10 × 3 mm, polished on one side. Polycrystals of zinc oxide were grown by laser molecular beam epitaxy on sapphire in Germany, dimensions 10 × 10 × 0.5 mm. The choice of these crystals is due to the fact that they all have a wide band gap and are characterized by ionic, ionic-covalent bonds, which allows us to study defect formation on the surface under the conditions of our experiment.

For the experimental realization of total current spectroscopy in its simplest configuration, a measuring circuit as depicted in Fig. 1 is indispensable [40]. A focused monokinetic electron beam (part 1 of Fig. 1) is directed towards the sample surface utilizing an electron-optical system (part 2 of Fig. 1). Within the region between the forming system and the planar sample (part 5 of Fig. 1), electrons traverse in a homogeneous retarding field, reaching the sample with an energy dictated by the displacement potential (U_d). The primary electron current (I_1) is established by the magnitude of the current generated between the electron gun's cathode and the sample under investigation. Upon interaction of primary electrons with the target, a fraction of them is reflected, yielding a current of secondary electrons (I_2), while the remainder penetrates the target, contributing to the overall current passing through the sample (I). The equilibrium of currents is expressed as follows [41]:

$$I_1 = I + I_2 \tag{1}$$

As the magnitude of the retarding field above the sample changes, the relative potentials of the electrostatic system remain constant. Consequently, the primary electron beam retains its focus, and the current I_1 remains constant in magnitude [42,43]. Taking this fact into consideration, it can be inferred that the magnitude of the secondary electron current I_2 can be assessed by measuring the current in the target circuit I:

$$I = I_1 - I_2 \; I_1 = const. \tag{2}$$

By applying a small (0.1 ÷ 0.2 V) sinusoidal voltage with a frequency of $\omega = 1000$ Hz to the cathode unit, it is possible to modulate the primary beam in energy, and using the synchrodetection system (6-part of Fig. 1) to isolate the first derivative of the current in the sample circuit. Then the expression for the current balance will be written as:

$$\frac{dI}{dE_p} = \frac{d(I_1 - I_2)}{dE_p} = -\frac{dI_2}{dE_p} = S(E_p) \tag{3}$$

To obtain total current spectra, an electron beam (part 1 of Fig. 1) with an energy of 0–600 eV (current ~10^{-9} A, half-width of the energy distribution of the electron beam 0.3 eV) is directed onto the surface of a zinc oxide crystal. The electron current density reached 5 × 10^{10} el/cm^2 per second, which led to a dose of 1.2 × 10^{14} el/cm^2 within 40 min. If we assume that there are about 1.09 × 10^{15} atoms per cm^2 on the ZnO surface, and that the electron energy when recording total current spectra is below the potential sputtering limit, then sputtering effects can be neglected. Also, the registration of the full current spectra takes place within 15–30 s, this is a very small dose, but enough to charge the surface. We have a working vacuum of approximately 10^{-8} Torr, this means approximately 10^{-8} mbars, then to obtain 1 monolayer of residual gas on the surface of zinc oxide it takes more than 1000 s (Table 1). If we assume that it takes more than 1000 s to obtain one monolayer of residual gas on the surface under our vacuum conditions, this means that the influence of the residual gas on the obtained data is very minimal, thus we can neglect the amount of residual gas under our experimental conditions.

The interpretation of the spectra of the total current of zinc oxide was

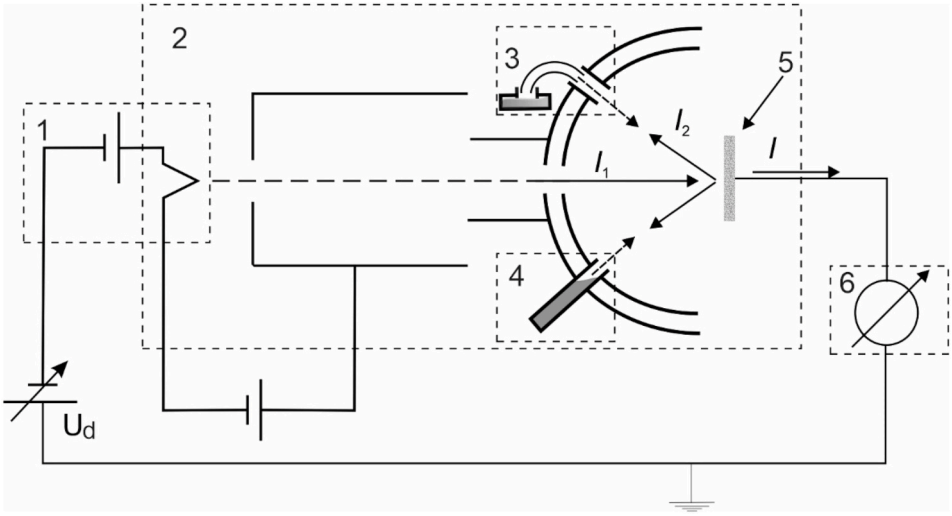

Fig. 1. Electrical circuit of the total current spectrometer, 1-electron gun, 2-electron-optical system, 3-ion gun, 4-evaporator, 5-substrate, 6-electronics for recording the integral current 10^{-8} A.

Table 1
Ultrahigh vacuum regimes.

Pressure	p (Torr)	$<10^{-8}$
Particle number density	n (cm^{-3})	$< 10^8$
Mean free path	λ (cm)	$> 10^6$
Impingement rate	Z_a ($cm^{-2} * s^{-1}$)	$< 10^{12}$
Vol.-related collision rate	Z_v ($cm^{-3} * s^{-1}$)	$< 10^8$
Monolayer time	τ (s)	>1000
Type of gas flow		Molecular flow

carried out on the basis of the energy diagram of the formation of the fine structure shown in Fig. 2. When the energy of the primary electron beam becomes high enough to excite various defects, the probability of primary electrons leaving the solid decreases, and a peak appears in the total current spectrum curve at the corresponding energy position of the defect. The primary peak in the total current spectra indicates the vacuum level and in all spectra the reference point is chosen (zero in Fig. 2.). Also, for convenience, shifts in the total current spectra due to changes in the potential and work function of the surface are not taken into account, since the level of defects relative to the vacuum level does not change.

Each current spectrum was recorded using a fixed set of ion irradiation doses. The primary peak in all curves indicates the beginning of the counted excitation energy of defects.

In this case, the occurrence of defects, their disappearance or their transformation into other types of defects was judged by changes in the intensity (*h*) and half-width of the corresponding peaks (Fig. 2).

The studies were carried out in films and single crystals of ZnO,

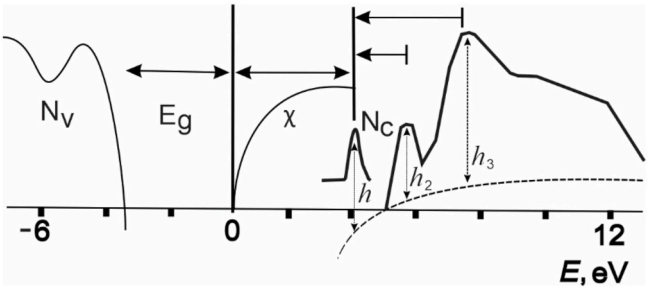

Fig. 2. Energy level diagram responsible electron transitions for the zinc oxide total current spectra fine structure.

under irradiation with slow electrons, up to a certain dose (D = 1.5 * 10^{13} el/cm^2) and energy (0–600 eV). The formation of defects and their effect on the negative charging of the surface of ZnO crystals were investigated. Some ZnO data obtained by total current spectroscopy have also been studied by other teams [44]. A detailed description of total current spectroscopy methods is given in Refs. [13,45–48].

The technique has an ion gun operating on an ionization mechanism to use surface cleaning and ion etching of samples [49]. All studies were carried out at room temperature. Surface cleanliness and elemental analysis was monitored using SIMS and total current spectra. To measure the temperature on the target surface, a chromel-alumel thermocouple was used in the temperature range (20 ÷ 1000 °C). A detailed description of SIMS methods is given in Refs. [46,50].

The nature of changes in the mass spectra of negative ion sputtering of ZnO depending on the etching time was studied using the method of secondary ion mass spectrometry. Temperature annealing can be used to clean the surface, but this may negatively affect the properties of the crystal. This procedure can lead to the formation of color centers, which negatively affects the research results. Therefore, to clean the surface, it is advisable to etch the surface of zinc oxide.

The results of studying the characteristics of changes in the mass spectra of ZnO depending on the time of etching with primary cesium ions (Fig. 3) showed that the surface of zinc oxide is covered with a dense layer of residual gas oxide and that even many hours of bombardment with primary cesium ions with an energy of 3 keV was insufficient to completely remove the oxide film from the surface. In this state, negative Zn- ions on the surface of zinc oxide constitute a significant proportion of the mass spectrum of negative ion sputtering, while at the same time, Znn-cluster ions are absent in the mass spectrum. Fig. 3 shows the mass spectrum of the products of negative ion sputtering of ZnO depending on the time of etching with primary cesium ions: a - without etching; c - after 4 h of etching with cesium ions with an energy of 3 keV.

With increasing etching time on the surface, the amount of zinc oxide generally increases - this means the lattice ion sputtering process, which shows the cleaned surface of zinc oxide. A zinc surface covered with a film of oxygen is ~300 times worse at sputtering than pure metallic zinc. Therefore, zinc oxide is one of the most spray-resistant materials. To obtain true values of the zinc sputtering coefficient, it is necessary to remove the oxide film from its surface. These studies showed that as the oxide film is removed from the zinc surface, a sharp change in negative ion sputtering occurs. As the etching time increases, the yield of negative Zn- ions decreases. This indicates that negative Zn- ions are knocked out

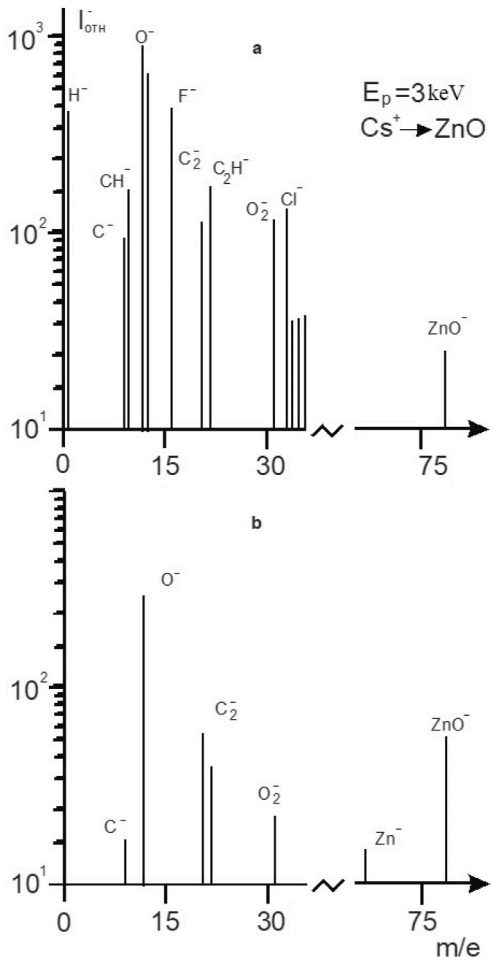

Fig. 3. Mass spectrum of products of negative ion sputtering of ZnO depending on the time of etching with primary cesium ions: a - without etching; c - after 4 h of etching with cesium ions with an energy of 3 keV.

not only from the crystal lattice, but also from chemical zinc compounds on the surface, in particular from the oxide film.

Under these bombardment modes, a decrease in Zn- ions is observed, and cluster ions appear in the mass spectrum of sputtering products, the yields of which depend on the current strength of the cesium ions. This increase in the Zn- yield becomes slower and reaches a stationary value. The distribution of the relative content of Zn- cluster ions depending on the number of zinc atoms in them is determined by the value of the affinity energy of these clusters. Thus, after obtaining a cleaned zinc oxide surface, further studies (electron irradiation) can be carried out to achieve the goal.

The preparation and cross-sectional (S)TEM measurements of polycrystalline and single-crystalline ZnO samples were carried out as follows. A study was conducted using (S)TEM cross-sections of polycrystalline and monocrystalline ZnO samples. For this, fragments were chipped from the crystalline samples using a diamond knife. The separated layers of the samples were carefully polished with an abrasive, and then a circular disk with a diameter of 5 mm was cut using the Ultrasonic Disk Cutter (model 170, Fischione Instruments, USA). For the final preparation of the sample for measurement, the obtained disk was polished, milled, and ion-milled at 10 keV using a precision ion polishing system (model 1051, Fischione Instruments, USA). Measurements (S)TEM-EDX were conducted at 200 keV using a transmission electron microscope with an EDX attachment (Talos-200i, Thermo Fisher Scientific, USA) and an EDX system (Bruker XFlash GTI 30, Bruker, Germany). A detailed description of the (S)TEM technique can be found in the works [51,52].

2.1. Computational method

We also carried out comparative studies using the computational method of density functional theory (DFT), which can confirm the results obtained by total current spectroscopy. All the calculations are performed using density functional theory with generalized gradient approximation (GGA) as implemented in the VASP codes [53,54]. We have employed the plane-wave DFT + U [55] methodology with the PBE [56] exchange-correlation functional. The GGA + U was used, and the U_{eff} value for the localized 3 d electrons of Zn is 10.5 eV and 2p orbital for the O atom is 7.5 eV. The selected U_{eff} value gives the closest match to the experimental electronic band gap of ZnO [57]. The energy cut-off for the plane wave basis set is kept as 500eV and Monkhorst–Pack 5 × 5 × 1 k-point mesh [58]. We have module ZnO(000 $\bar{1}$) surface and 2 × 2 × 1 supercell in which the bottom ZnO layers are fixed while the top ZnO layers are allowed to relax. Dipole corrections are adapted to compensate for interactions between slabs [59]. Structure relaxation progresses until the forces on atoms are less than 0.01 eV/Å. Slabs and vacuum are increased to four ZnO layers and 15 Å, respectively [60]. Details about the DFT method can be found in the following works [61,62].

3. Results and discussion

Comparative studies were carried out and the total current spectra of poly and single ZnO crystals were obtained (Fig. 4). The first peak in the total current spectrum (peak α) is called the "primary". It appears if the energy of the primary electron beam becomes equal to the energy position of the minimum of unoccupied electron states (DOUS - Density of Unoccupied States), and the probability of electron penetration into the solid appears [63,64].

As can be seen from the total current spectra, at electron energies of 4.2 eV (peak α), the excitation of interband transitions begins for both samples, which indicates the transition of electrons from the potential barrier to the conduction band, or in other words, the electrochemical potential, or also called electron affinity (for metals - work function). The difference in the total current spectra of the two samples is that the intensities of the peaks at 3.5 eV (Fig. 4, peak γ) and 8 eV (peak δ) are more weakly reflected in polycrystalline ZnO. There is also a weak formation of several peaks at excitation energies of 10 eV, 16 eV, 22 eV, which, according to data obtained from studies using ab initio calculations based on DFT [65], is shown in Fig. 5. As you can see, this figure more clearly represents the excitation of interband transitions from the total current spectra of zinc oxide crystals. As can be seen, the total current spectra show in more detail the band gap, electron affinity energy or surface work function (primary peak energy), unoccupied states above the Fermi level, and local states. Some peaks are consistent with

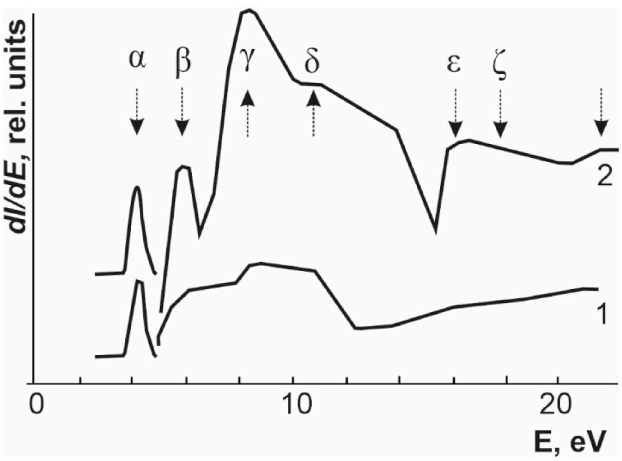

Fig. 4. Total current spectra of poly (1) and single crystals (2) of zinc oxide.

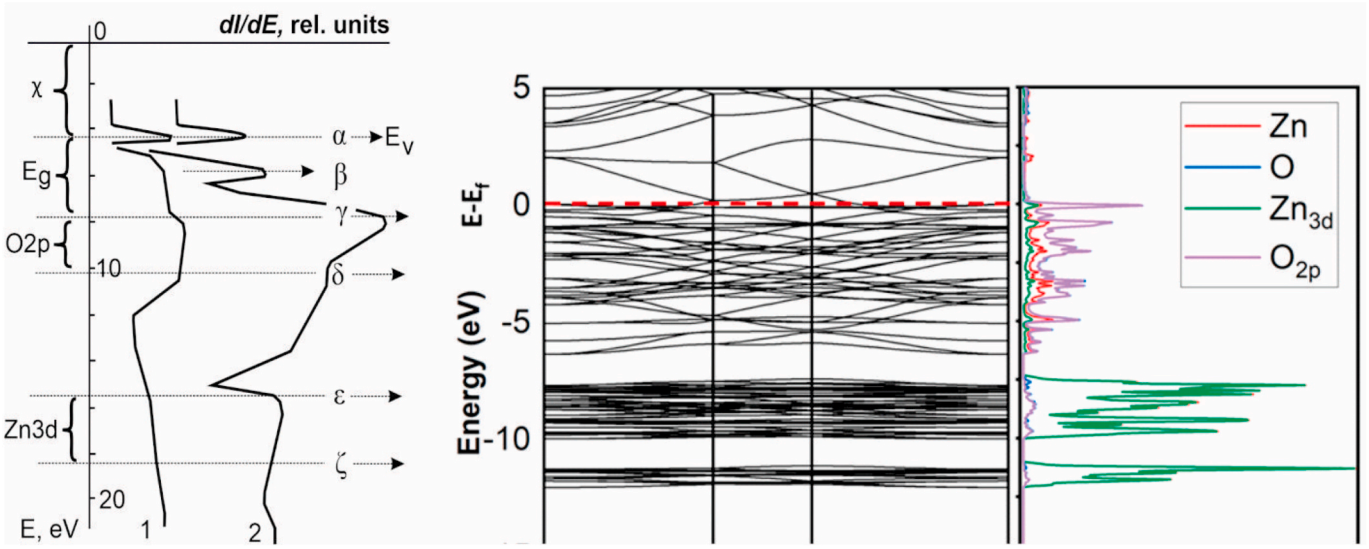

Fig. 5. Comparison of total current spectra of zinc oxide crystals with DFT calculations (1-polycrystal, 2-single crystal).

the energy states of bands in the near-surface region observed in DFT calculations [66]. For example, according to DFT calculations and total current spectra, we see that the first peak (Figs. 4 and 5, peak γ) at an electron energy of 7.5 eV in the energy axis (relative to the primary peak - 3.2 eV) is associated with the excitation of O2p electrons - states from the occupied valence band to unoccupied states in the conduction band, that is, the transition of an electron from the top of the valence band (VBM-valence band maximum) to the bottom of the conduction band of the zinc oxide sample (CBM-conduction band minimum). The second δ peak at 10.5 eV probably results from electron excitation of small O2p states from the lower energy of the occupied valence band to the free conduction band. The third largest peak ε at a photon energy of 16 eV (relative to the primary peak - 12 eV) is attributed to the excitation electron from the 3 d states of Zn from the occupied valence band to the unoccupied conduction band.

When comparing the obtained data from total current spectroscopy and DFT Fig. 5, one can notice with the naked eye that the 2p state of oxygen and the 3 d state of zinc and other levels coincide when the spectra are added to each other. As illustrated in Fig. 5, the valence band maximum (VBM) is predominantly contributed by the 2p orbitals of O atoms in the 0–5 eV range, indicating that oxygen atoms are active on the ZnO (000 $\bar{1}$) surface. In contrast, the contribution from the 3 d orbitals of Zn atoms is significantly lower, positioned well below the Fermi level (approximately −6 eV to −12 eV), suggesting that Zn atoms are strongly bound to the ZnO (000 $\bar{1}$) surface.

Thus, the occurrence of peaks at an energy of 3.5 eV (Fig. 4, peak γ) relative to the primary peak shows the band gap - E_g. It is also clear from the spectrum that in the band gap there is a peak at an energy of 1.8–2.0 eV (Fig. 4, peak β), which shows the presence of local states - oxygen vacancies on the surface of the sample. Also, from the spectrum we can say that on a polycrystalline sample this peak is wider (peak β - oxygen vacancies) than on a single-crystalline zinc oxide. This indicates a high concentration of surface defects of oxygen vacancies.

Analysis of the total current spectra of two crystals shows that, in a polycrystalline sample, the intensity of the peaks is very weak, due to electron scattering in the polycrystalline lattice. Also, the peak at an energy of 7.5 eV in the total current spectrum of single-crystal ZnO shows the presence of oxygen atoms at the interface with the surface, which indicates the polar orientation (000 $\bar{1}$) of ZnO [67,68]. The basal planes of the crystal (0001) and (000 $\bar{1}$) are polar. The (0001) plane corresponds to the surface bounded by zinc cations (Zn–ZnO), the (000 $\bar{1}$) plane – by oxygen anions (O–ZnO) [69]. Computational calculations obtained by the DFT method also showed that the surface is limited by oxygen atoms, which confirms the experimental data obtained by total current spectroscopy (Fig. 6).

In previous work examining the energy dependence of zinc oxide, we showed that each resulting total current spectrum shifts toward higher energies, indicating the formation of a negative charge on the surface of the zinc oxide [12]. Fig. 7 shows several spectra from previous work to explain the current data. Curve 1 shows the spectrum of the total current of zinc oxide without irradiation. Curve 2 shows the spectrum of the total current of zinc oxide after irradiation with electrons with an energy of 10 eV. In this case (within 1 min) a dose = $1.5\text{-}10^{13}$ el/cm^2 is collected on the sample. This dose was sufficient to saturate the charging on the surface, since increasing the dose did not lead to other noticeable changes on the surface of the sample. As noticeable, the spectrum has shifted to the right by about 5 eV. Further, an increase in energy by 20 eV (curve 3) leads to a shift in the spectrum by 9–10 eV. And so on, before irradiation at energies of 115 eV, the surface potential increases to 43 eV. Further, when irradiated with electrons with an energy of 120 eV, the surface potential drops sharply to 18–20 eV and decreases to 7–8 eV at irradiation energies of 150 eV. Further, with an increase in the energy of the primary electrons, the potential of the surface of zinc oxide does not decrease or increase. The thick dashed arrow shows the

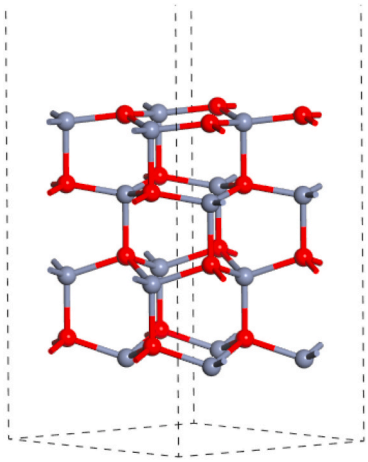

Fig. 6. Schematic representation of optimized polar ZnO (000 $\bar{1}$) surface obtained using our DFT method, zinc atoms are represented by gray spheres, oxygen atoms are represented by red spheres.

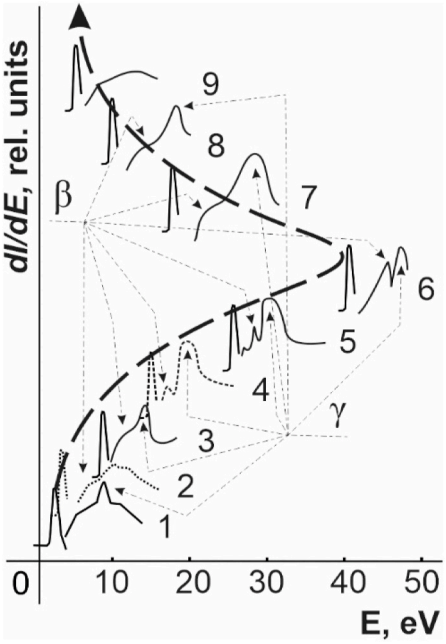

Fig. 7. Total current spectra of single-crystal zinc oxide under irradiation with slow electrons.

direction of shift of the primary peak. This is the value of the generated potential of the surface of zinc oxide.

Curves: 1 - total current spectra of the cleaned surface of zinc oxide single crystals after annealing at a temperature of 400 °C; 2 - total current spectra when irradiated by electrons with energy E_{ir} – 10 eV; 3–20 eV; 4–40 eV; 5–50 eV; 6–75 eV; 7–100 eV; 8–120 eV; 9–130 eV; 10–150 eV;

Fig. 8 clearly shows the dependence of the change in the negative surface potential of poly and single-crystalline zinc oxide samples on the energy of electron irradiation.

As can be seen, the value of the negative charge accumulated on the surface increases to 43 eV, after the irradiation energy of the primary electrons 120 eV begins to fall, but the negative potential on the surface does not disappear and remains at the level of 7 eV. It is also clear from the figure that the negative potential on the surface of poly and single crystal zinc oxide behaves differently. More negative potential accumulates on a polycrystalline sample than on a single-crystalline sample. This is probably due to the crystallographic orientation of atoms and their clusters on the surface or morphology. Taking morphological patterns of the surface of poly and single crystal zinc oxide can bring some clarity to the effects we observed associated with the accumulation of potential on the surface.

In previous Figs. 4, 5 and 7, we mentioned the formation of oxygen vacancies (β peak) upon electron irradiation. From the obtained total current spectra, it became clear that pre-radiation vacancies are observed on the surface of zinc oxide and their formation after irradiation with electrons. If we trace their kinetic, energy and temperature dependence, we get the following Figs. 9–11.

Fig. 9 shows the energy dependence of the relative intensity of the 2.0 eV peak - an oxygen vacancy on the surface of a ZnO crystal on the energy of electron irradiation. As can be seen, before irradiation with electrons with an energy of 20 eV, the intensity of the vacancy peak does not increase significantly. This indicates the existence of pre-radiation defects on the surface of zinc oxide. With an increase in energy by 20 eV, there is a sharp jump in intensity by about 2 times, which can be attributed to the formation of vacancies due to electron irradiation. The energy region of the site can be divided into two: 1 and 2 region of electron irradiation. The first region involves vacancies that already exist (pre-radiation) on the surface of zinc oxide; here the electron energy is not enough to create vacancies.

In the second region of the irradiation section, both pre-radiation and vacancies formed during irradiation with electrons with an energy of 20 eV are involved. Further, an increase in the energy of electron irradiation does not lead to an increase in the formation of oxygen vacancies, which indicates the threshold for the formation of oxygen vacancies on the surface of the zinc oxide crystal. Thus, it is clear from the graph that an irradiation energy of 20 eV for zinc oxide is the threshold for the formation of defects on the surface; below this energy, electrons cannot create electron-hole pairs.

Fig. 10 shows the temperature dependence of the relative intensity of the 2.0 eV peak – an oxygen vacancy on the surface of a ZnO crystal. As can be seen, with an increase in temperature from room temperature to 300 °C, the intensity of the 2.0 eV peak does not change noticeably, which is not a characteristic behavior for vacancies. A similar situation was observed by Hoffman in his studies [70], where grown bulk ZnO crystals annealed in vacuum in zinc and oxygen vapor were characterized using optical and magnetic resonance spectroscopy. Experiments showed that the concentration of residual carriers is due to residual oxygen vacancies in the material. Annealing samples at a temperature of about 1000 °C reduces the concentration of H donors and oxygen vacancies by one order of magnitude. Photoluminescence and DLTS results suggest emission at 2.45 eV (green band) and a donor level at 530 meV below the conduction band, which is associated with a doubly charged oxygen vacancy. The results indicate negative charging of oxygen vacancy defects predicted by theoretical calculations.

From the temperature dependence we can say that oxygen vacancies are not annealed up to 300 °C.

Fig. 11 shows the kinetics of the relative intensity of the 2.0 eV peak – an oxygen vacancy on the surface of a ZnO crystal. As can be seen, the intensity of the 2.0 eV peak—oxygen vacancy—drops by two times within 4 h, by five times within 8 h, and then the kinetics of vacancies does not change noticeably. Only in this way can the concentration of oxygen vacancies on the surface be reduced, but it is impossible to completely remove vacancies from the surface.

Thus, it is clear from the graphs that the detected peak of 2.0 eV in the total current spectrum actually belongs to oxygen vacancies on the surface of the zinc oxide crystal. It reacts very stable to temperature and annealing time.

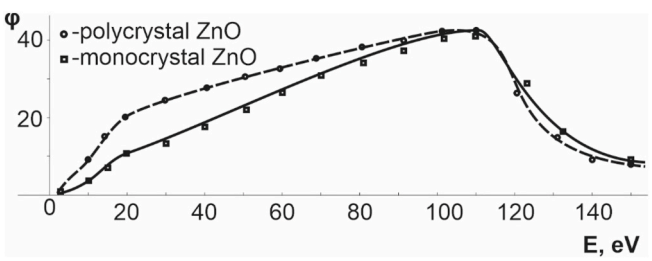

Fig. 8. Dependence of the change in the negative potential of the surface of poly and single crystal ZnO on the energy of electron irradiation. cu.

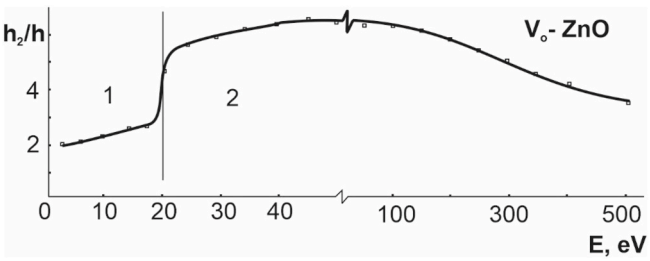

Fig. 9. Energy dependence of the relative intensity of the 2.0 eV peak – oxygen vacancy on the surface of a ZnO crystal under electron irradiation.

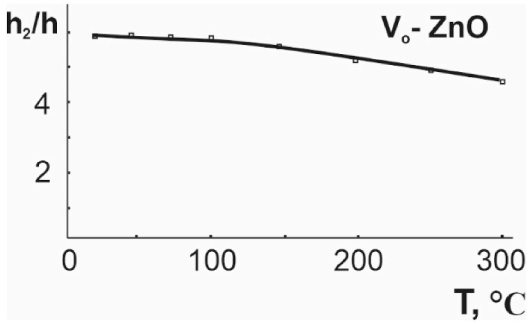

Fig. 10. Temperature dependence of the relative intensity of the 2.0 eV peak – oxygen vacancy on the surface of a ZnO crystal.

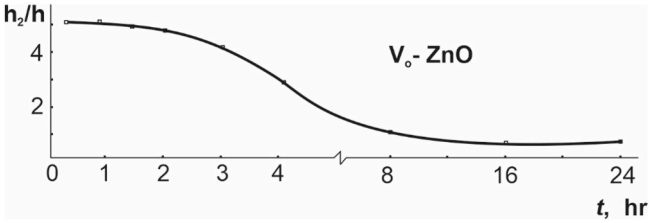

Fig. 11. Kinetics of the relative intensity of the 2.0 eV peak – oxygen vacancies on the surface of a ZnO crystal.

Our experiments show that in the case of electron irradiation of the ZnO surface in the energy range $1 \leq E \leq 20$ eV, negative charging of the surface occurs due to dissociative processes occurring below the ionization and excitation thresholds, which can only occur due to dissociative electron attachment. In this case, the formation of a negative charge due to the capture of electrons by pre-radiation oxygen vacancies. This process is considered temporary and resonant; during relaxation, the electron is simply ejected, leaving the hole in an excited state. It should be noted that the formation of charging on the surface occurs at energies below the energy of the sample band gap; this is probably due to pre-radiation vacancies.

The increase in the concentration of vacancies on the surface of zinc oxide at irradiation energies of 20 eV (Fig. 9) may be associated with the ionization potential of oxygen and zinc atoms. Experimentally determined [71–74], to displace an atom from a cell node from the volume, at least energy must be expended:

$$E_{disp} = 3*E_{pi} \quad (4)$$

here E_{disp} is the energy expended for displacement the atom, E_{pi} is the ionization potential of the atom (Table 2). On the surface (20.4 eV) this value is two times less than in the bulk ($13.6*3 = 40.8$), since the strength of the attachment of an atom in a lattice site depends on the number of bonds, and on the surface some of them are broken. In other words, E_{pi} is less than the threshold displacement energy E_{disp}, which characterizes the formation of post-ionization defects in the volume. It seems that the electron energy is sufficient to break the bonds of the ZnO cluster into positive Zn^+ and negative O^- ions, which leads to the formation of a double-layer charge on the surface. The results show that the formed double-layer charging region on the outer side of the surface is covered with negative oxygen ions (Fig. 12).

Table 2
Ionization levels of zinc and oxygen (eV).

ionization potential (eV)	Zn	O
1	9.39	13.6
2	17.9	35.1
3	39.7	54.9
4	59.5	77.4
5	82.6	113.9
6	107.9	138.1
7	133.9	739.2

We know that ZnO is a partially ionic crystal, and therefore its double layers consist of positively negatively charged Zn and O ions. To date, a two-layer model of surface charging under electron bombardment of a dielectric target has been developed [18,21,75], according to which, a layer of positive or negative charge is formed due to the emission of secondary electrons. It is also clear from our data that the ZnO (000 $\bar{1}$) substrate has a surface with high reactivity (the surface is limited by oxygen ions), which, when irradiated with electrons, leads to the formation of an additional charge barrier layer, creating a potential.

Also, to compare the experiment, we carried out additional studies using transmission electron microscopy. An (S)TEM study was carried out on a cross section of a polycrystalline ZnO sample (Fig. 13a). Analytical mapping of the Zn and O elements of the polycrystalline ZnO sample was also carried out using (S)TEM/EDX (Fig. 13b and c).

The sample consists of many irregularly shaped grains, the sizes of which vary from a few nanometres to several micrometres. The grains border each other to form boundaries that are often jagged and tortuous. The grains have a hexagonal wurtzite structure, which was confirmed by interatomic distances in the crystal structure in (S)TEM photographs (Fig. 13a). Moreover, the c-axis of the grains is oriented in different directions, which leads to the formation of a polycrystalline structure. Photograph 1a shows some defects, such as dislocations and pores, which can affect material properties such as strength and electrical conductivity. Elemental mapping of the area demonstrates that the sample is composed of Zn atoms (Fig. 13b) and oxygen atoms (Fig. 13c). The sample consists of zinc oxide, and no other elements were detected that could form other zinc compounds. A cross-section of a single-crystal ZnO sample was also studied, showing the structure of the material at the atomic level (Fig. 14).

A (S)TEM photograph of a single crystal sample shows monolithic grain, which means that the sample consists of a single crystal (Fig. 14a). The grain has an irregular shape, close to rectangular. The grain size is not determined, but the image shows that it is quite large. There are no grain boundaries, since the sample is single-crystalline. The photographs show some defects such as dislocations and pores. Dislocations are a line of discontinuity in the crystal lattice, and pores are voids in the material. (S)TEM photograph of a single crystal sample of a monolithic grain, meaning that the sample consists of a single crystal. The grain has an irregular shape, close to rectangular. The grain size is not determined, but the image shows that it is quite large. There are no grain boundaries, since the sample is single-crystalline. The photographs show some defects such as dislocations and pores. Dislocations are a line of discontinuity in the crystal lattice, and pores are voids in the material. Elemental mapping in (S)TEM/EDX photographs shows that the red atoms are oxygen and the green atoms are zinc (Fig. 14b). This is confirmed by the fact that the sample is composed of Zn and O atoms, since it is zinc oxide.

4. Conclusions

The influence of low-energy electrons ($E = 0 \div 600$ eV) on the surface of zinc oxide crystals has been studied. In our opinion, low-energy electron irradiation of the surface of zinc oxide crystals stimulates three types of dissociative processes that occur directly as a result of inelastic collisions of electrons with surface anions and cations. These reactions cause physical and chemical processes through dissociation, breaking

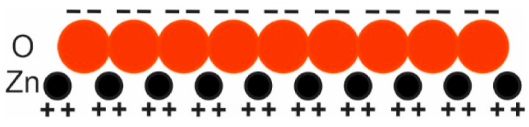

Fig. 12. Two-layer model of surface charging during electron bombardment of a semiconductor target.

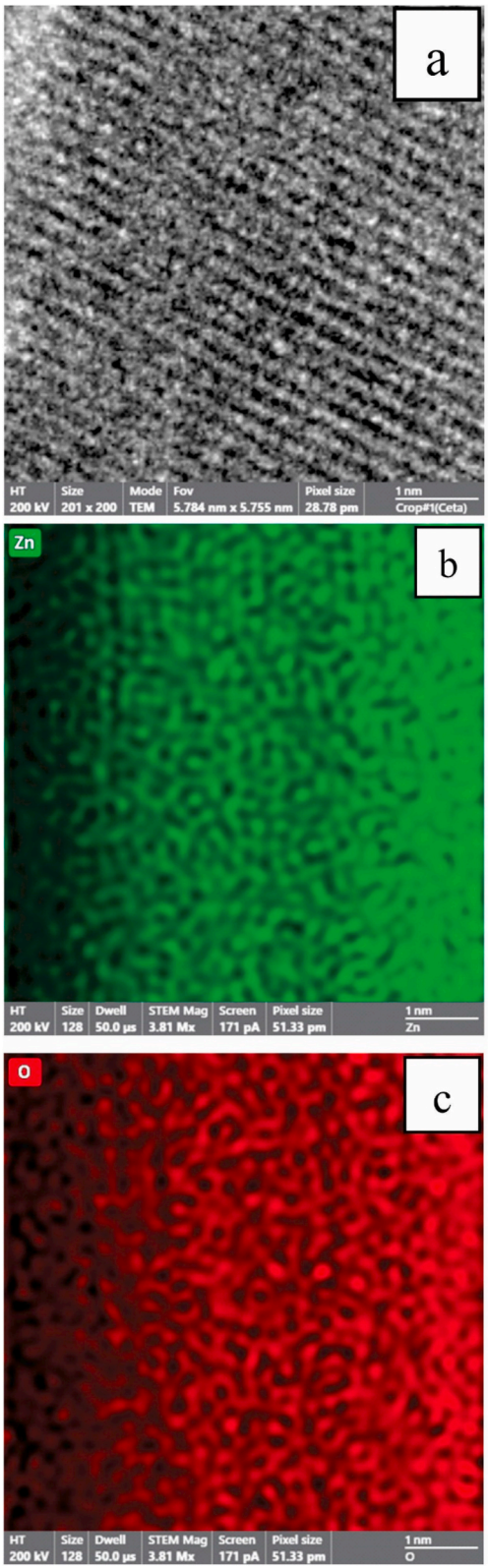

Fig. 13. (S)TEM cross-sectional image of a polycrystalline ZnO sample (a). Analytical mapping of Zn (b) and O (c) elements of a polycrystalline ZnO sample using (S)TEM/EDX.

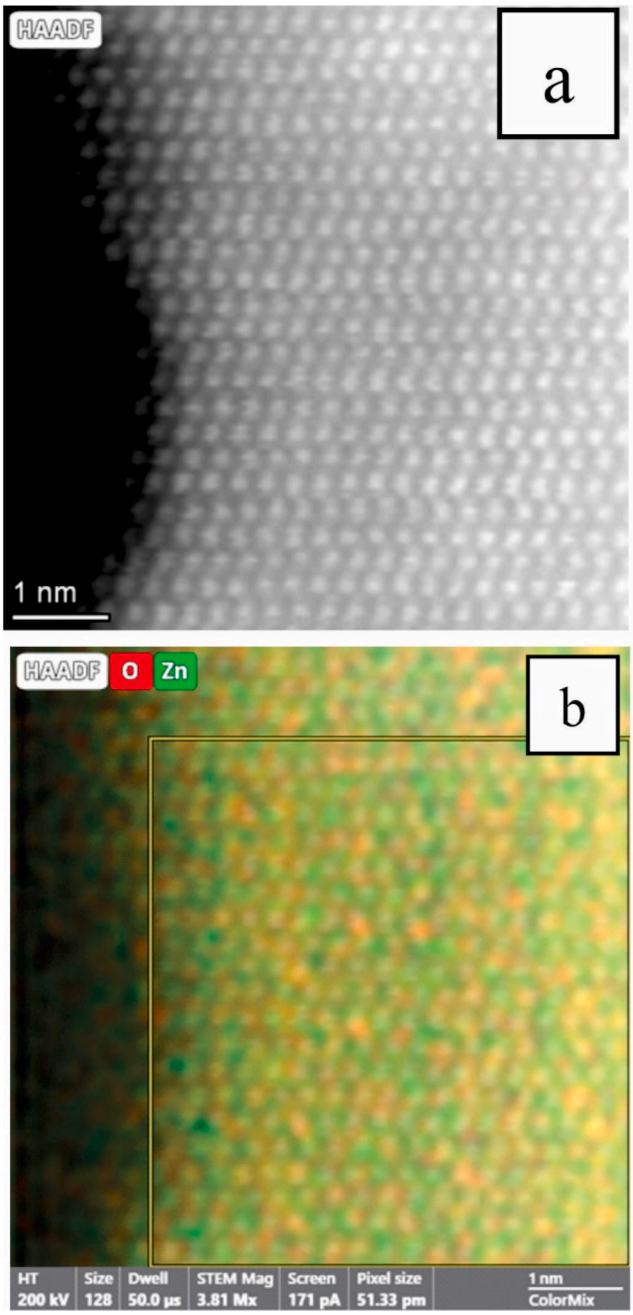

Fig. 14. (S)TEM photographs of a cross section of a single crystalline ZnO sample (a), Analytical mapping of Zn and O elements of a polycrystalline ZnO sample using (S)TEM/EDX (b).

and formation of bonds, and atomic and molecular rearrangement of the surface of the sample. As shown, the energy of the primary electron is of paramount importance and can determine what types of primary processes can be activated on the zinc oxide surface.

In the first case, in the energy range 1eV $\leq$ E $\leq$ 20eV, negative charging of the ZnO surface occurs due to dissociative electron attachment to pre-radiation oxygen vacancies.

In the second case, in the energy range 20 eV $\leq$ E $\leq$ 120 eV, an increase in negative charging is observed due to the breaking of the bonds of the ZnO cluster into positive Zn+ and negative O- ions, which leads to the formation of a two-layer charge on the surface, on the outer side of the surface covered with negative oxygen ions. The energy threshold for the formation of an anion vacancy (~20 eV) on the ZnO surface was determined.

In the third case, at energies above E ≥ 120 eV, the negative charge on the ZnO surface decreases, possibly due to oxygen ESD and other secondary electronic processes.

The data obtained from the presented work can be used to control ions and chemical reactions at the molecular level, as well as to obtain epitaxial two-dimensional thin-film heterostructures using surface potential [76]. It is safe to say that if the surface is charged during film growth, it will have a very large impact not only on the morphology of the deposited surface, but also on the structural perfection of the resulting films [77]. Also, the results of charging that we discovered occurring on the surface of zinc oxide can be used to interpret the processes occurring on the surface of spacecraft, where in the upper layers of the earth's atmosphere the charge value reaches 20 keV.

Ethics approval and consent to participate

Not applicable.

Consent for publication

Not applicable.

Availability of data and material (data transparency)

The data that support the findings of this study are available from the corresponding author upon reasonable request.

Conflicts of interest/Competing interests

The authors report no conflicts of interest include appropriate disclosures. The authors alone are responsible for the content and writing of this article.

Funding

This research was supported by Ministry of Science and Higher Education of the Russian Federation, project 124041700069-0 granted to Penza State University. This research received no other grant from any funding agency in the public, commercial, or not-for-profit sectors.

Disclosure of potential conflicts of interest

Not applicable.

Research involving human participants and/or animals

Not applicable.

Informed consent

Not applicable.

CRediT authorship contribution statement

All authors contributed to the research conception and design manuscript.

Conceptualization, Data curation, Material preparation, Data collection and analysis: were performed by Utkirjon Sharopov, Muzaffar Kurbanov and Aleksei Komolov.

Formal analysis, Investigation, Methodology, Resources, Software, Validation, Visualization, Vacuum preparing and ion etching: Muzaffar Kurbanov, Mukhtorjon Karimov, Dilmurod Saidov, Feruza Akbarova, Sitora Turopova.

Writing - original english version draft preparation: Utkirjon Sharopov, Kamoliddin Samiev, Feruza Akbarova, Sitora Turopova.

Funding acquisition, Resources: Utkirjon Sharopov, Kamoliddin Samiev, Akbarjon To'raev, Kulwinder Kaur, Zafar Iskandarov, Sokhib Islamov, Aleksei Komolov, Igor Pronin.

Supervision: Utkirjon Sharopov, Kulwinder Kaur, Aleksei Komolov.

Software, Validation: Obtained results of electronic levels and surface states were discussed and agreed with professor Kulwinder Kaur, Marutheeswaran Srinivasan, Aleksei Komolov.

Writing – review & editing, ((S)TEM/EDX results): Hanna Bandarenka, Odiljon Abdurakhmonov, Sherzod Abdurakhmonov, Kulwinder Kaur, Marutheeswaran Srinivasan.

All authors read and approved the final manuscript.

Declaration of competing interest

The authors declare that they have no known competing financial interests or personal relationships that could have appeared to influence the work reported in this paper.

Data availability

No data was used for the research described in the article.

Acknowledgements

Equipment of the Research Park of St. Petersburg State University, "Physical methods of surface investigation" was used within the research presented in the article. The explores of samples using (S)TEM and (S)TEM-EDX was carried out at the Tashkent Institute of Chemical Technology in the laboratory "Physical-chemical methods of nanomaterials analysis" on a Talos-200i facility.

References

[1] A. Ait hssi, et al., A DFT theoretical and experimental study of the effect of indium doping within electrochemical deposited ZnO, Vacuum 217 (Nov. 2023) 112503, https://doi.org/10.1016/j.vacuum.2023.112503.

[2] I. Maglevanny, V. Smolar, The constructive procedure for solving the problems of electron transport in the multi-layer specimens for the normally incident electron beam. 1. Solution of the model transport equations for a point beam : energy and charge deposition, Vacuum 46 (11) (Nov. 1995) 1261–1269, https://doi.org/10.1016/0042-207X(95)00010-0.

[3] A. Studer, D.P. Curran, The electron is a catalyst, Nat. Chem. 6 (9) (Sep. 2014) 765–773, https://doi.org/10.1038/nchem.2031.

[4] A. Sytchkova, et al., Impact of proton irradiation on photoluminescent properties of C-doped ZrO2 films prepared by ALD, Vacuum 224 (Jun. 2024) 113083, https://doi.org/10.1016/j.vacuum.2024.113083.

[5] K.M. Karimberganovich, et al., Low energy Ar+ ion scattering on InGaP(001) surface, e-Journal Surf. Sci. Nanotechnol. 18 (Apr. 2020) 164–167, https://doi.org/10.1380/ejssnt.2020.164.

[6] L. Sala, I.B. Szymańska, C. Dablemont, A. Lafosse, L. Amiaud, Response under low-energy electron irradiation of a thin film of a potential copper precursor for focused electron beam induced deposition (FEBID), Beilstein J. Nanotechnol. 9 (Jan. 2018) 57–65, https://doi.org/10.3762/bjnano.9.8.

[7] C.R. Arumainayagam, H.-L. Lee, R.B. Nelson, D.R. Haines, R.P. Gunawardane, Low-energy electron-induced reactions in condensed matter, Surf. Sci. Rep. 65 (1) (Jan. 2010) 1–44, https://doi.org/10.1016/j.surfrep.2009.09.001.

[8] E.H.H. Hasabeldaim, S.G. Menon, H.C. Swart, R.E. Kroon, Electron beam irradiation studies of ZnGa2O4:Mn2+ green phosphor, Vacuum 192 (Oct. 2021) 110447, https://doi.org/10.1016/j.vacuum.2021.110447.

[9] E. Böhler, J. Warneke, P. Swiderek, Control of chemical reactions and synthesis by low-energy electrons, Chem. Soc. Rev. 42 (24) (2013) 9219, https://doi.org/10.1039/c3cs60180c.

[10] S.A. Pshenichnyuk, et al., Microsecond dynamics of molecular negative ions formed by low-energy electron attachment to fluorinated tetracyanoquinodimethane, J. Chem. Phys. 155 (18) (Nov. 2021) 184301, https://doi.org/10.1063/5.0072264.

[11] U. Sharopov, et al., Formation of defects on the surface of LiF crystals under irradiation with different ions mass, Radiat. Eff. Defect Solid (Oct. 2022) 1–14, https://doi.org/10.1080/10420150.2022.2133716.

[12] U.B. Sharopov, B.G. Atabaev, R. Djabbarganov, Defect Formation on the surface of ZnO using low-energy electrons, J. Surf. Investig. X-ray, Synchrotron Neutron Tech. 14 (1) (Jan. 2020) 101–104, https://doi.org/10.1134/S1027451020010164.

[13] U.B. Sharopov, et al., Comparison of electron irradiation on the formation of surface defects in situ and post thin-film LiF/Si(111) deposition, Thin Solid Films 735 (Oct. 2021) 138902, https://doi.org/10.1016/j.tsf.2021.138902.

[14] N. Cornet, et al., Electron beam charging of insulators with surface layer and leakage currents, J. Appl. Phys. 103 (6) (Mar. 2008) 064110, https://doi.org/10.1063/1.2890427.
[15] R.R. Jalolov, S.Z. Urolov, Z.S. Shaymardanov, S.S. Kurbanov, B.N. Rustamova, Complex features of the photoluminescence from ZnO nanorods grown by vapor-phase transport method, Mater. Sci. Semicond. Process. 128 (Jun. 2021) 105783, https://doi.org/10.1016/j.mssp.2021.105783.
[16] A.A. Bhat, et al., Band-gap alteration of Zn2SnO4 nanostructures for optical and photo-luminescent applications, Mater. Chem. Phys. 306 (Sep. 2023) 127993, https://doi.org/10.1016/j.matchemphys.2023.127993.
[17] I.A. Pronin, et al., Chemical binding of carbon dioxide on zinc oxide powders prepared by mechanical milling, Inorg. Mater. 57 (11) (Nov. 2021) 1140–1144, https://doi.org/10.1134/S0020168521110108, 2021 5711.
[18] K.E. Ozerova, A.A. Tatarintsev, E.I. Rau, K.F. Minnebaev, S.V. Zaitsev, Differences in the kinetic characteristics of charging ferroelectrics and dielectrics upon ion irradiation, Bull. Russ. Acad. Sci. Phys. 85 (8) (Sep. 2021) 835–840, https://doi.org/10.3103/S1062873821080190, 2021 858.
[19] E.I. Rau, et al., Second crossover energy of insulating materials using stationary electron beam under normal incidence, Nucl. Instrum. Methods Phys. Res. Sect. B Beam Interact. Mater. Atoms 266 (5) (Mar. 2008) 719–729, https://doi.org/10.1016/J.NIMB.2007.12.093.
[20] E.I. Rau, A.A. Tatarintsev, E.Y. Zykova, K.E. Markovets, Ozerova, K.F. Minnebaev, Charging of dielectrics under ion irradiation, Vacuum 177 (Jul. 2020) 109373, https://doi.org/10.1016/J.VACUUM.2020.109373.
[21] Y. Ding, K.C. Pradel, Z.L. Wang, In situ transmission electron microscopy observation of ZnO polar and non-polar surfaces structure evolution under electron beam irradiation, J. Appl. Phys. 119 (1) (Jan. 2016) 015305, https://doi.org/10.1063/1.4939618.
[22] A.A. Borzunov, D.V. Lukyanenko, E.I. Rau, A.G. Yagola, Reconstruction algorithm of 3D surface in scanning electron microscopy with backscattered electron detector, J. Inverse Ill-Posed Probl. 29 (5) (Oct. 2021) 753–758, https://doi.org/10.1515/JIIP-2020-0136/MACHINEREADABLECITATION/RIS.
[23] T. Krasta, I. Manika, A. Kuzmin, J. Maniks, R. Grants, A.I. Popov, Effect of ion-induced secondary radiations on the formation of extended defects and radiolysis beyond the range of swift 12C, 50Ti, and 52Cr ions in LiF, Nucl. Instrum. Methods Phys. Res. Sect. B Beam Interact. Mater. Atoms 545 (Dec. 2023) 165142, https://doi.org/10.1016/j.nimb.2023.165142.
[24] M. Bai, D.S. Pickard, C. Tanasa, M.A. McCord, C.N. Berglund, R.F.W. Pease, Resist charging in electron-beam lithography, 18th Annu. BACUS Symp. Photomask Technol. Manag. 3546 (Dec. 1998) 383, https://doi.org/10.1117/12.332874.
[25] S.S.A. An, et al., Physicochemical properties of surface charge-modified ZnO nanoparticles with different particle sizes, Int. J. Nanomed. 41 (Dec) (2014), https://doi.org/10.2147/IJN.S57923.
[26] E.I. Rau, A.A. Tatarintsev, E.Y. Zykova, Influence of ion implantation and electron pre-irradiation on charging of dielectrics under electron beam irradiation: application to SiO2, Nucl. Instrum. Methods Phys. Res. Sect. B Beam Interact. Mater. Atoms 460 (Dec. 2019) 141–146, https://doi.org/10.1016/J.NIMB.2018.12.030.
[27] S.K. Höeffgen, S. Metzger, M. Steffens, Investigating the effects of cosmic rays on space electronics, Frontiers. Phy. 8 (Sep. 18, 2020), https://doi.org/10.3389/fphy.2020.00318. Frontiers Media S.A.
[28] Y. Zheng, et al., Space radiation and plasma effects on satellites and aviation: quantities and metrics for tracking performance of space weather environment models, Sp. Weather 17 (10) (Oct. 2019) 1384–1403, https://doi.org/10.1029/2018SW002042.
[29] E.V. Shirshneva-Vaschenko, P.S. Shirshnev, Z.G. Snezhnaia, L.A. Sokura, V. E. Bougrov, A.E. Romanov, Zinc oxide aluminum doped slabs for heat-eliminating coatings of spacecrafts, Acta Astronaut. 163 (Oct. 2019) 107–111, https://doi.org/10.1016/j.actaastro.2019.07.005.
[30] B.E. Egamberdiev, et al., Influence of doping with rare earth elements on the parameters of silicon photocells, Appl. Sol. Energy 58 (4) (Aug. 2022) 490–496, https://doi.org/10.3103/S0003701X22040065.
[31] A.G. Komilov, B.E. Egamberdiev, R. Kabulov, Y.Z. Nasrullayev, F.A. Akbarov, The result of successive exposure to reverse and forward bias on the electrophysical characteristics of ZnO:Al/i-ZnO/CdS/CuIn1 – xGax(S, Se)2/Mo structure solar cells, Appl. Sol. Energy 58 (4) (Aug. 2022) 476–481, https://doi.org/10.3103/S0003701X22040090.
[32] B.E. Egamberdiev, N.T. Rustamov, A.S. Mallaev, A.M. Norov, Effect of annealing on the crystal structure of the surface of silicon doped with Ni, Fe, and Co ions, J. Surf. Investig. 9 (3) (May 2015) 612–615, https://doi.org/10.1134/S1027451015030222.
[33] M.K. Karimov, F.O. Kuryozov, S.R. Sadullaev, M.U. Otabaev, S.B. Bobojonova, Investigation of defect InP(001) surface by low energy ion scattering spectroscopy, Mater. Sci. Forum 1049 (Jan. 2022) 192–197. https://doi.org/10.4028/www.scientific.net/MSF.1049.192.
[34] E.B. Buzok, S. Yalcin, G. Demircan, D. Yılmaz, B. Aktas, E. Aytar, The structural, optical, electrical and radiation shielding properties of Co-doped ZnO thin films, Radiat. Phys. Chem. 222 (Sep. 2024) 111840, https://doi.org/10.1016/j.radphyschem.2024.111840.
[35] M.M. Mikhailov, A.N. Sokolovskiy, S.A. Yuryev, V.V. Karanskiy, Synergistic effects in the change in optical properties of ZnO powder modified with SiO2 nanoparticles upon sequential irradiation with electrons and solar quanta, Adv. Space Res. 66 (11) (Dec. 2020) 2703–2710, https://doi.org/10.1016/j.asr.2020.08.020.
[36] I.T. Martin, K. Crowley, A.F. Hepp, Thin-film materials for space power applications, in: Photovoltaics for Space: Key Issues, Missions and Alternative Technologies, Elsevier, 2022, pp. 215–263, https://doi.org/10.1016/B978-0-12-823300-9.00015-7.
[37] J. Yang, J. Hu, Y. Ye, J. Xu, Y. Hu, R. Shen, Design, preparation, and characterization of a novel ZnO/CuO/Al energetic diode with dual functionality: logic and destruction, Def. Technol. 34 (Apr. 2024) 57–68, https://doi.org/10.1016/j.dt.2023.09.017.
[38] S.A. Komolov, L.T. Chadderton, Total current spectroscopy, Surf. Sci. 90 (2) (Dec. 1979) 359–380, https://doi.org/10.1016/0039-6028(79)90350-9.
[39] P. Hashir, P. Pradyumnan, A.F. Wani, K. Kaur, Experimental and first-principles thermoelectric studies of bulk ZnO, IOP Conf. Ser. Mater. Sci. Eng. 1263 (1) (Oct. 2022) 012025, https://doi.org/10.1088/1757-899x/1263/1/012025.
[40] A.S. Komolov, et al., Density of the unoccupied electronic states of the ultrathin films of the aziridinylphenylpyrrol substituted fullerene, J. Electron. Spectrosc. Relat. Phenom. 205 (Nov. 2015) 52–56, https://doi.org/10.1016/j.elspec.2015.08.002.
[41] A.S. Komolov, et al., Conduction band electronic states of ultrathin layers of thiophene/phenylene co-oligomers on an oxidized silicon surface, J. Electron. Spectrosc. Relat. Phenom. 235 (Aug. 2019) 40–45, https://doi.org/10.1016/j.elspec.2019.07.001.
[42] V.E. Henrich, Fast, accurate secondary-electron yield measurements at low primary energies, Rev. Sci. Instrum. 44 (4) (Apr. 1973) 456–462, https://doi.org/10.1063/1.1686155.
[43] S.A. Pshenichnyuk, A. Modelli, N.L. Asfandiarov, E.F. Lazneva, A.S. Komolov, Electron stimulated ring opening in diphenylphthalide dicarboxylic acid: its likely role in the unique properties of phthalide-based materials, J. Chem. Phys. 151 (21) (Dec. 2019) 214309, https://doi.org/10.1063/1.5130152.
[44] A.S. Komolov, et al., Density of unoccupied electronic states of the ultrathin layers of dibromo-bianthracene on the surface of layer-by-layer grown ZnO, Crystallogr. Rep. 69 (1) (Feb. 2024) 109–113, https://doi.org/10.1134/S1063774523601223.
[45] R. Djabbarganov, B.G. Atabaev, Z.A. Isakhanov, U.B. Sharopov, Energy threshold of the atomic and cluster sputtering of some elements under bombardment with Cs, Rb, and Na ions, J. Surf. Investig. X-ray, Synchrotron Neutron Tech. 13 (4) (Jul. 2019) 640–643, https://doi.org/10.1134/S1027451019040049.
[46] U.B. Sharopov, B.G. Atabaev, R. Djabbarganov, M.K. Kurbanov, M.M. Sharipov, Procedure for determining defects in sputtered clusters of ionic crystals, J. Surf. Investig. X-ray, Synchrotron Neutron Tech. 10 (1) (Jan. 2016) 245–249, https://doi.org/10.1134/S1027451016010328.
[47] U. Sharopov, et al., Comparative research fluorine and colloidal aggregate formation on the surface lithium fluoride thin films during electronic, ionic and thermal treatments, Vacuum 213 (Jul. 2023) 112133, https://doi.org/10.1016/j.vacuum.2023.112133.
[48] A.S. Komolov, P.J. Møller, E.F. Lazneva, Interface formation between oligo (phenylele–vinylene) films and highly ordered pyrolytic graphite and Ge(1 1 1) surfaces, J. Electron. Spectrosc. Relat. Phenom. 131–132 (Oct. 2003) 67–75, https://doi.org/10.1016/S0368-2048(03)00104-X.
[49] U.B. Sharopov, K. Kaur, M.K. Kurbanov, D.S. Saidov, E.T. Juraev, M.M. Sharipov, Controlling the low-temperature ionic purification of a silicon surface by electron spectroscopy, Silicon 14 (9) (Jul. 2022) 4661–4667, https://doi.org/10.1007/s12633-021-01268-0.
[50] U. Sharopov, et al., Influence of the irradiation of ions of different mass on the formation of surface defects of lithium fluoride thin films, Surf. Interface Anal. 54 (10) (Jun. 2022) 1052–1059, https://doi.org/10.1002/sia.7130.
[51] O.E. Abdurakhmonov, U.B. Sharopov, S.E. Abdurakhmonov, Z.C. Kadirova, New method of chemical synthesis for nanostructured Nd-Fe-B alloy, J. Magn. Magn Mater. 589 (Jan. 2024) 171562, https://doi.org/10.1016/j.jmmm.2023.171562.
[52] O. Abdurakhmonov, et al., Production of High-Coercive nanostructured Nd-Fe-B alloy by chemical method, J. Magn. Magn Mater. 600 (Jun. 2024) 172130, https://doi.org/10.1016/j.jmmm.2024.172130.
[53] G. Kresse, J. Hafner, Ab initio molecular dynamics for open-shell transition metals, Phys. Rev. B 48 (17) (Nov. 1993) 13115–13118, https://doi.org/10.1103/PhysRevB.48.13115.
[54] G. Kresse, J. Furthmüller, Efficient iterative schemes for ab initio total-energy calculations using a plane-wave basis set, Phys. Rev. B Condens. Matter 54 (16) (Oct. 1996) 11169–11186, https://doi.org/10.1103/PhysRevB.54.11169.
[55] X. Ma, Y. Wu, Y. Lv, Y. Zhu, Correlation effects on lattice relaxation and electronic structure of zno within the GGA+ U formalism, J. Phys. Chem. C 117 (49) (Dec. 2013) 26029–26039, https://doi.org/10.1021/jp407281x.
[56] J.P. Perdew, K. Burke, M. Ernzerhof, Generalized gradient approximation made simple, Phys. Rev. Lett. 77 (18) (Oct. 1996) 3865–3868, https://doi.org/10.1103/PhysRevLett.77.3865.
[57] Ü. Özgür, et al., A comprehensive review of ZnO materials and devices, J. Appl. Phys. 98 (4) (Aug. 2005) 041301, https://doi.org/10.1063/1.1992666.
[58] H.J. Monkhorst, J.D. Pack, Special points for Brillouin-zone integrations, Phys. Rev. B 13 (12) (Jun. 1976) 5188–5192, https://doi.org/10.1103/PhysRevB.13.5188.
[59] L. Bengtsson, Dipole correction for surface supercell calculations, Phys. Rev. B Condens. Matter 59 (19) (May 1999) 12301–12304, https://doi.org/10.1103/PhysRevB.59.12301.
[60] G. Kresse, O. Dulub, U. Diebold, Competing stabilization mechanism for the polar ZnO(0001)-Zn surface, Phys. Rev. B 68 (24) (Dec. 2003) 245409, https://doi.org/10.1103/PhysRevB.68.245409.
[61] S.A. Khandy, I. Islam, K. Kaur, A.M. Ali, A.F.A. El-Rehim, Electronic structure, stability, photocatalytic and optical properties of new lead-free double perovskites Tl2PtX6 (X = Cl, Br) for light-harvesting applications, Mater. Chem. Phys. 297 (Mar. 2023) 127293, https://doi.org/10.1016/j.matchemphys.2023.127293.

[62] S.A. Khandy, J. Da Chai, Strain engineering of electronic structure, phonon, and thermoelectric properties of p-type half-Heusler semiconductor, J. Alloys Compd. 850 (Jan. 2021) 156615, https://doi.org/10.1016/j.jallcom.2020.156615.
[63] A.S. Komolov, et al., Structure of vacant electronic states of an oxidized germanium surface upon deposition of perylene tetracarboxylic dianhydride films, Phys. Solid State 58 (2) (Feb. 2016) 377–381, https://doi.org/10.1134/S106378341602013X.
[64] S.A. Komolov, Total Current Spectroscopy of Surfaces, Gordon and Breach Science, Philadelphia, 1992 [Online]. Available: https://books.google.co.uz/books/about/Total_Current_Spectroscopy_of_Surfaces.html?id=p9QQI962g4YC&redir_esc=y.
[65] S.A. Khandy, Inspecting the electronic structure and thermoelectric power factor of novel p-type half-Heuslers, Sci. Rep. 11 (1) (Oct. 2021) 20756, https://doi.org/10.1038/s41598-021-00314-6.
[66] A.F. Wani, B. Rani, U.B. Sharopov, S. Dhiman, K. Kaur, Thermoelectric investigation of transition metal oxide NiO2: a first principles study, Int. J. Energy Res. 46 (6) (Feb. 2022) 8527–8535, https://doi.org/10.1002/er.7741.
[67] K. Mun Wong, S.M. Alay-e-Abbas, Y. Fang, A. Shaukat, Y. Lei, Spatial distribution of neutral oxygen vacancies on ZnO nanowire surfaces: an investigation combining confocal microscopy and first principles calculations, J. Appl. Phys. 114 (3) (Jul. 2013) 034901, https://doi.org/10.1063/1.4813517.
[68] P.J. Møller, S.A. Komolov, E.F. Lazneva, "A total current spectroscopy study of metal oxide surfaces: I. Unoccupied electronic states of ZnO and MgO," [Online]. Available: http://iopscience.iop.org/0953-8984/11/48/315, 1999.
[69] K. Jacobi, G. Zwicker, A. Gutmann, Work function, electron affinity and band bending of zinc oxide surfaces, Surf. Sci. 141 (1) (Jun. 1984) 109–125, https://doi.org/10.1016/0039-6028(84)90199-7.
[70] X. Li, J. Song, Y. Liu, H. Zeng, Controlling oxygen vacancies and properties of ZnO, Curr. Appl. Phys. 14 (3) (Mar. 2014) 521–527, https://doi.org/10.1016/j.cap.2014.01.007.
[71] D.R. Locker, J.M. Meese, Displacement thresholds in ZnO, IEEE Trans. Nucl. Sci. 19 (6) (1972) 237–242, https://doi.org/10.1109/TNS.1972.4326839.
[72] J. Meese, D. Locker, Oxygen displacement energy in ZnO, Solid State Commun. 11 (11) (Dec. 1972) 1547–1550, https://doi.org/10.1016/0038-1098(72)90517-0.
[73] K. Lorenz, E. Alves, E. Wendler, O. Bilani, W. Wesch, M. Hayes, Damage formation and annealing at low temperatures in ion implanted ZnO, Appl. Phys. Lett. 87 (19) (Nov. 2005), https://doi.org/10.1063/1.2126137.
[74] A.N. Dudin, V.Y. Yurina, FORMATION OF FRENKEL PAIRS IN ZnO, SiO_2, AND Al_2O_3 UNDER THE ACTION OF ELECTRON AND PROTON IRRADIATIO, Messenger AmSU 97 (97) (2022) 47–53, https://doi.org/10.22250/20730268_2022_97_47.
[75] A. Melchinger, S. Hofmann, Dynamic double layer model: description of time dependent charging phenomena in insulators under electron beam irradiation, J. Appl. Phys. 78 (10) (Nov. 1995) 6224–6232, https://doi.org/10.1063/1.360569.
[76] J. Houplin, C. Dablemont, L. Sala, A. Lafosse, L. Amiaud, Electron processing at 50 eV of terphenylthiol self-assembled monolayers: contributions of primary and secondary electrons, Langmuir 31 (50) (Dec. 2015) 13528–13534, https://doi.org/10.1021/acs.langmuir.5b02109.
[77] M.S. Moumita Ghosh, Electron beam assisted zinc nanocrystal growth from ZnO nanorod, Mater. Sci. (2023), https://doi.org/10.26434/chemrxiv-2023-v3v1x.